Epitaxial 2D SnSe2/ 2D WSe2 van der Waals heterostructures

Aretouli, KE, Tsoutsou, D, Tsipas, P, Marquez-Velasco, J, Aminalragia Giamini, S, Kelaidis, N, Psycharis, V & Dimoulas, A

Original citation & hyperlink:
Aretouli, KE, Tsoutsou, D, Tsipas, P, Marquez-Velasco, J, Aminalragia Giamini, S, Kelaidis, N, Psycharis, V & Dimoulas, A 2016, 'Epitaxial 2D $SnSe_2$/ 2D WSe_2 van der Waals heterostructures' *ACS Applied Materials and Interfaces*, vol 8, no. 35, pp. 23222-23229
https://dx.doi.org/10.1021/acsami.6b02933

DOI 10.1021/acsami.6b02933
ISSN 1944-8244
ESSN 1944-8252

Publisher: American Chemical Society

Epitaxial 2D $SnSe_2$/ 2D WSe_2 van der Waals heterostructures for near broken gap Tunneling Field Effect Transistors

K. E.Aretouli[1, 2], D. Tsoutsou[1], P. Tsipas[1], J. Marquez-Velasco[1,3], S. A. Giamini[1, 2], N. Kelaidis[1], A. Dimoulas[1]*

[1]*Institute of Nanoscience and Nanotechnology, National Center for Scientific Research "DEMOKRITOS", 15310, Athens, Greece*

[2]*University of Athens, Department of Physics, Section of Solid State Physics, 15684 Athens, Greece*

[3]*National Technical University of Athens, Department of Physics, 15780 Athens, Greece*

KEYWORDS: 2D semiconductors, $SnSe_2$, WSe_2, van der Waals heterostructures, Molecular beam epitaxy, tunneling field effect transistors

ABSTRACT

Van der Waals heterostructures of 2D semiconductor materials can be used to realize vertical tunneling field effect transistors (TFETs), which potentially allow high currents in the on-state for low power/high performance applications. It is shown in this work that high quality $SnSe_2/WSe_2$ vdW heterostructure can be grown by molecular beam epitaxy on

AlN(0001)/Si(111) substrates using a Bi_2Se_3 buffer layer. A valence band offset of 0.8 eV, matches the energy gap of $SnSe_2$ in such a way that the VB edge of WSe_2 and the CB edge of $SnSe_2$ are lined up, making this materials combination suitable for (nearly) broken gap 2D-2D TFETs.

INTRODUCTION

The subthreshold slope (SS) in conventional transistors is limited by thermionic transport over a potential barrier to values which are larger than 60 mV/decade. Transport through a tunnel barrier in tunneling field effect transistors (TFETs) [1] can help overcome this fundamental limitation and obtain steep slope devices (SS<60 mV/dec) operating at very low power supply voltage. In homojunction TFET transistors produced in the form of a gated p-i-n structure [1, 2] interband tunneling occurs through a large barrier, limiting the transistor on-current (I_{ON}) in the on-state. Staggered or broken gap III-V heterostructure TFETs [3] offer lower and thinner tunneling barriers allowing for larger I_{ON}. However, heteroepitaxial defects induce trap assisted tunneling which increases I_{OFF}, converts transport to thermionic and degrades performance. On the other hand, 2D metal dichalcogenide semiconductor heterostructures (HS) weakly coupled through van der Waals (vdW) interactions are free of dangling bonds and create the prospect for uninhibited current transport through the interface, which makes them good candidates for vertical heterojunction TFETs. A recent work [4] presents the first 2D/3D TFET which is fabricated by placing an exfoliated two-layer MoS_2 (2D) on bulk Ge (3D) substrates. Although subthermionic transport at remarkably low bias of 0.1 V is obtained, I_{ON} is rather small. By making a 2D/2D TFET using vdW HS of 2D semiconductors, it could be possible to overcome the problem of low I_{ON}. Indeed, the large variety of MX_2 materials (M= Mo, W, V, Nb, Sn, Ti, Zr, Hf, Re and X=S, Se, Te) with different band gaps, electron affinities

(EA) and workfunctions (WF) allows the fabrication of HS with type III band alignment which could lead to (nearly) broken gap TFETs. In such case, the tunneling occurs through the ultrathin (0.3-0.35 nm) vdW gap creating the prospect of large I_{ON}. According to theoretical predictions [5], type III HS can be formed by combining group IVB (Hf, Zr) with group VIB (Mo, W) metal dichalcogenides due to the large difference in WF (or EA) between the two classes of materials. Experimental studies [6] of the $HfSe_2/MoSe_2$ candidate combination however reveal type II HS with small (~ 0.13 eV) valence band offset, which is attributed [6] to the observed [7, 6] small $HfSe_2$ WF of 5.5 eV [6] and small WF difference between $HfSe_2$ and $MoSe_2$ [6] in contrast to theoretical predictions [5]. An interesting alternative combination involving $WSe_2/SnSe_2$ vdW HS has been proposed [8] on the basis of device modeling predicting ultra-small SS ~14 mV in a near broken-gap configuration supported by early experimental findings of molecular beam epitaxy (MBE)-grown $SnSe_2$ on bulk WSe_2 [9]. Recently it has been shown that tin diselenide can be used for the fabrication of a number of devices such as Esaki tunnel diodes when combined with phosphorene [10], supercapacitor [11] photodetector [12] and field effect transistor devices [13-14] all based on exfoliated flakes.

While most of the research device work is based on small layers exfoliated from bulk, large area epitaxial growth (e.g. by MBE) is required for real world applications. Following early pioneering MBE work [15, 16, 17, 9], more recently, the MBE growth of WSe_2 [18, 19] and other 2D semiconductors ($MoSe_2$ [20, 21, 22], $HfSe_2$ [7]) is reported on "friendly" 2D substrates like HPGO, graphene, and exfoliated MoS_2 substrates. On the other hand, MBE growth on bulk (3D) substrates, although challenging, it is technologically very important. Wurtzite epi-AlN(0001)/Si(111) substrates which are available in 300 mm wafer sizes at low cost are suitable for up scaling growth to large area wafers allowing processing

according to industry standards for volume production. Following our previous work on the MBE growth of $MoSe_2$, $HfSe_2$, $ZrSe_2$, $TaSe_2$ and their vdW HS on AlN/Si substrates [23, 24, 25] we extend our investigations here on the growth of WSe_2 and $SnSe_2$ and their vdW HS on the same substrates with and without a Bi_2Se_3 buffer layer. While epitaxial WSe_2 has been studied to some extent [18, 19], the epitaxy of $SnSe_2$ is not known in sufficient detail. Unlike most transition metals which have only one oxidation state forming stoichiometric diselenide compounds, Sn has two oxidation states (+2 and +4) so except from the diselenide, the monoselide phase is also possible in several polytypes (orthorhombic *Pnma* and *Cmcm* and the rock-salt) [26, 27] which introduce complexity in the growth efforts and device design. While using CVD methodologies [28, 29, 30, 31] it is possible to control the growth of the different Sn selenide phases and polytypes, it may not be easy to do the same with MBE. Moreover, $SnSe_2$ has been reported in two different crystal structures, namely the 2H with D_{6h} (P63/mmc) symmetry and the CdI_2-type 1T phase with D_{3d} (P-3m1) symmetry (S1), although it is not clear which one is the most stable and most frequently observed. In the present paper optimal growth conditions and substrates are employed demonstrating high quality 1T-$SnSe_2$ phase in combination with WSe_2 in a vdW epitaxial configuration targeting vertical TFET device layer structures.

EXPERIMENTAL SECTION

The epitaxial growth of WSe_2 and $SnSe_2$ thin films performed by Molecular Beam Epitaxy (MBE) on AlN/Si(111) substrates. Initially the substrates were chemically cleaned to remove residual surface organic contaminants and then an *in-situ* degassing followed at 730°C in the MBE chamber. High purity metals W and Sn were evaporated from e-gun evaporator whereas Bi and Se were evaporated from k-effusion cells. WSe_2 and $SnSe_2$ epilayers were grown under Se rich conditions with a growth rate of 1 ML/30sec. Deposited samples were structurally and physically characterized by means of *in-situ*

Reflection High Energy Electron Diffraction (RHEED), Raman, X-ray Photoelectron Spectroscopy (XPS) and Angle-Resolved Photoemission Spectroscopy (ARPES) techniques. Raman spectroscopy was performed using a 514.5 nm laser beam with a power of ~1.2mW. XPS spectra were collected with a PHOIBOS 100 (SPECS) hemispherical analyzer, at a pass energy of 15 eV. The take-off angle was set at 37° relative to the sample surface. Gaussian-Lorentzian shapes (Voigt functions) were used for deconvolution of the recorded spectra after standard Shirley background subtraction. ARPES measurements were carried out using a 2D-CCD detector and a He excitation source with He I radiation at 21.22 eV. The energy resolution of the system was better than 40 meV. Photoelectrons emitted by the samples are measured in the energy distribution curve (EDC) mode with a with polar angle step of 1°. The Density–Functional Theory (DFT) calculations were performed using the Vienna Ab Initio Simulation Package [32] and projector-augmented waves. The generalized-gradient approximation (GGA) [33] with Perdew–Burke–Ernzerhof (PBE) [34] parameterization was used as exchange correlation functional. To include vdW corrections, the semi-empirical DFT-D3 Grimme's method [33] was applied. Self-consistent force optimizations were performed until the Hellmann-Feynman force between the atoms converged to $5x10^{-5}$eV/Å. The energy cutoff was set at 500 eV, while the Monkhorst-Pack scheme [35] with a k-point grid of 15x15x1 was chosen. Calculation of the band structure with and without SOC were performed, using for these calculations k-mesh 31 k-point per symmetric line along KΓM direction.

RESULTS AND DISCUSSION

Raman scattering results

Each one of tin and tungsten selenide materials is first grown directly on AlN/Si substrates. Using high Se overpressure such that the evaporation rate ratio is Se/Sn ~15/1, a dominant $SnSe_2$ phase is obtained at an optimum temperature of 225 ^oC, which is well below the temperature of 270 ^oC at which the material is found to be thermally unstable dissociating in UHV. On the other hand the growth of WSe_2 on AlN/Si proceeds in two steps. First, a 4ML WSe_2 is deposited at 490^oC followed by post deposition annealing at 670^oC in order to improve the surface ordering and crystallinity. The Raman spectra of $SnSe_2$ and WSe_2 are shown in Fig. 1(a) and (b), respectively. In Fig. 1(a) two dominant peaks at 186.27 cm^{-1} and 112 cm^{-1} agree well with the out of plane A_{1g} and in-plane E_g components, respectively, as previously reported [12, 14] for 1T $SnSe_2$ films with the D_{3d} symmetry, exfoliated from bulk. A rich Raman spectrum is observed (Fig. 1(b)) for WSe_2 featuring two pronounced peaks at 249 and 259 cm^{-1} which can be assigned to E^1_{2g} (in-plane) and A_{1g} (out of plane) modes of 2H-WSe_2 [36] and a number of second order peaks in agreement with results reported for bulk chemical vapor transport (CVT)-grown 2H-WSe_2 [37].

Epitaxial orientation probed by reflection high energy electron diffraction

The RHEED patterns (Fig 2(a)) indicate that there is a preferential azimuthal alignment between the $SnSe_2$ or WSe_2 epilayers and the substrate, however, it can be inferred from the diffused diffraction streaks that the films are of inadequate crystalline quality. Then, a good quality 5 QL Bi_2Se_3 buffer layer was first grown epitaxially on AlN [38] followed by $SnSe_2$

growth at 200 ^{o}C and a top layer WSe_2 (Fig 2(b)) at T=210^{o}C. Growth in reverse order is also performed where a WSe_2 layer is first grown at T=250^{o}C on Bi_2Se_3 buffer, followed by a top $SnSe_2$ layer at T=225^{o}C (Fig. 2(c)). It should be noted that the growth is necessarily kept at low temperature because of the instability of Bi_2Se_3 and $SnSe_2$ layers at higher temperatures. The Bi_2Se_3 template improves substantially the crystalline quality of both the $SnSe_2$ and WSe_2 epilayers as can be seen from the sharper diffraction streaks in Figs. 2(b) and (c). It can be seen from the same figures that all layers, are azimuthally aligned despite their large lattice mismatch (a(Bi_2Se_3)=4.14 Å, a($SnSe_2$)=3.81 Å, a(WSe_2)=3.28 Å) [38, 39, 40], indicating vdW epitaxial growth for all three layers independent of the growth order. It is also evident from the RHEED pattern that the tin selenide adopts an hexagonal structure which excludes the possibility to have a monoselenide (SnSe) phase with the orthorhombic crystal structure.

Electronic Band Structure Imaging by ARPES

The electronic band structure of 4 ML $SnSe_2/Bi_2Se_3$/AlN/Si is imaged by ARPES and compared with DFT band structure calculations of CdI_2-$SnSe_2$ phase with D_{3d} symmetry as shown in Fig. 3. With the exception of minor details (see discussion below) a very good agreement between the experiment (Fig. 3(a)) and theory (Fig. 3(c)) is observed along two different crystallographic directions of high symmetry (Fig. 3(b)), indicating oriented films of good crystalline quality, confirming also the predominant growth of the 1T-$SnSe_2$ phase. It should be noted that the 2H-$SnSe_2$ with D_{6h} symmetry and the orthorhombic SnSe phase (*Pnma*) have distinctly different band structure (S2 supplementary), which does not match the experimental results (fig. 3(a)). Although the conduction band (CB) cannot be observed in the image of Fig. 3(a), a closer look at the line scan (Fig. 3(d)) obtained at a wavevector k_x =0.9A^{-1} corresponding to the M-point of the surface Brillouin Zone (BZ), reveals a weak peak near the Fermi energy, exactly where the CB minimum (CBM) is expected according

to theory (Fig. 3(c)). We attribute this weak peak to the onset of photoemission as the Fermi level crosses the bottom of the CB. Our claim is further supported by the enhanced contrast image presented in supplementary information (S3) showing a faint photoemission signal from the CB at the M point. By comparing with the line scan at the k_x=0 (Γ-point), we infer an indirect energy gap E_g of ~ 0.8eV. It should be noted that the experimental valence band maximum (VBM) is found to be at the Γ point (Fig. 3(a) and (d)) which differs from theoretical results according to which the VBM is predicted to be at a point between Γ and M, near Γ (Fig 3(c) and ref. 11).The experimental E_g value is substantially larger compared to theoretically predicted E_g~ 0.4 eV (Fig. 3(c)) which is attributed to the well-known problem of band gap underestimation by DFT. The experimentally determined E_g in this work is also slightly smaller than the experimentally reported value of ~1 eV [41-43] which may be attributed to different physical properties of our films grown by MBE. The Fermi level (Fig. 3(d) and S2) is located at -or just above- the bottom of the conduction band, indicating a strongly n-type material, which is in fair agreement with previous reports of unintentionally n-type doped $SnSe_2$ [13,41,44] although the origin of the unintentional doping is unknown.

Band lineups

The band alignments of $SnSe_2/WSe_2$ heterostructure on Bi_2Se_3/AlN/Si substrates were investigated and found to be nearly independent of the growth order between the $SnSe_2$ and WSe_2 on Bi_2Se_3. Below we present our band alignment analysis for the heterostructure which is grown in the order shown in Fig. 2(b) (First $SnSe_2$ grown on Bi_2Se_3, then WSe_2 grown on top). The WSe_2 is first grown thin (~1 ML) and the thickness is sequentially increased up to 8ML. The band alignment configuration does not change as the thickness increases.

The energy position of the core levels and the valence band maxima obtained from photoelectron spectroscopy data (Fig. 4 (a-c)), are used to determine the HS valence and conduction band offsets (VBO, CBO) according to Kraut's method [45] using the following expressions.

$$VBO = \left(E_{W4f7/2} - VBM\right)_{WSe2} + (E_{Sn3d5/2} - E_{W4f7/2})_{SnSe2/WSe2} - \left(E_{Sn3d5/2} - VBM\right)_{SnSe2}$$

$$CBO = \left(E_g\right)_{WSe2} - \left(E_g\right)_{SnSe2} + VBO$$

From (1), the VBO is estimated to be 0.8 eV. Accordingly, from (2) the CBO value is calculated to be 1.6-1.3 eV, using WSe_2 band gap energy values E_g in the range of 1.3-1.6 eV as reported in the literature [8,46,47] and $SnSe_2$ E_g of 0.8 eV, as measured in the present work (Fig. 3(d)). A slightly smaller CBO value of 1.4-1.1 eV is obtained, taking into account the literature reported band gap value E_g~1 eV for $SnSe_2$ [41-43]. Finally, the workfunctions (WF) are measured from the low energy electron cut-off in the UPS spectra (Fig. 4(d)) and found to be 5.35 eV and 5.1 eV for $SnSe_2$ and WSe_2, respectively. The constructed band alignment at the WSe_2/$SnSe_2$ heterointerface is given in Fig. 4(e). The Fermi level is well aligned through the heterointerface as expected for two layers in thermodynamic equilibrium, while it is found to be located about 0.3 eV above the WSe_2 VBM and only about 0.07 eV above the $SnSe_2$ CBM in accordance with the observed VB edge (Fig. 4(a-b)) and CB edge positions (Fig. 3(d)). The vacuum level is positioned with respect to the Fermi level taking into account the measured work functions and is found to be nearly the same in both sides of the heterostructure, yielding electron affinities χ=3.8-4.1 eV and 5.43-5.23 eV for WSe_2 and $SnSe_2$ close to previously published experimental values [9]. The small difference δ_{vac}~ 0.11 V in the vacuum level indicates a nearly ideal heterostructure with little charge transfer and very small dipole moment built at the interface. In good agreement with predictions [8], WSe_2/$SnSe_2$ HS forms a broken or near

broken gap band alignment depending on the E_g ($SnSe_2$) used, yielding ΔE_{CV}~0-0.2 eV (Fig. 4(e)). This could be an ideal situation for the TFET operation since with very small negative gate voltage applied on the WSe_2 side, the VB of WSe_2 can be raised above the CB of $SnSe_2$ producing a large band to band tunneling current through the ultrathin vdW gap, turning the TFET on. The complete device layer structure analyzed in this work is schematically illustrated in S4 (supplementary information). As evident from the discussion above, the Bi_2Se_3 buffer layer is necessarily introduced here in order to ensure a good crystalline quality of the heterostructure. However Bi_2Se_3 is conductive, since it is low gap (0.3 eV) material and being a topological insulator it possesses metallic surface states [38], therefore Bi_2Se_3 can serve as a bottom electrode in TFET device implementation.

CONCLUSIONS

In this work $SnSe_2/WSe_2$ van der Waals heterostructures are epitaxially grown by MBE on technologically important AlN(0001)/Si(111) substrates using a thin Bi_2Se_3 buffer layer to improve the crystal quality of the layers. Although tin selenide can be found in different crystal structures and stoichiometries, optimized growth conditions are employed in this work to obtain single phase material, namely the 1T-$SnSe_2$ polytype. This phase, as grown by MBE, has an indirect energy gap around 0.8 eV while the Fermi level is located at the conduction band edge indicating a strongly n-type unintentionally doped semiconductor. On the other hand, the MBE-grown 2H WSe_2 is unintentionally p-type doped semiconductor with the Fermi level lying about 0.3 eV above the valence band maximum. When the two materials are combined, the conduction and valence band edges of $SnSe_2$ and WSe_2, respectively, are lined up in a (nearly) broken gap configuration implying that band to band tunneling through an ultrathin van der Waals gap can be switched on and off easily

upon application of a small bias across the interface. This defines an ideal device layer structure for the implementation of 2D-2D vertical TFETs.

AUTHOR INFORMATION

Corresponding Author

*a.dimoulas@inn.demokritos.gr

Author Contributions

The manuscript was written through contributions of all authors. All authors have given approval to the final version of the manuscript.

Funding Sources

ERC Advanced Grant SMARTGATE-291260.

Acknowledgements: This work is supported by the ERC Advanced Grant SMARTGATE-291260. The authors thank Dr. G. Kordas for making the Raman set up available to us for measurements and IMEC for providing the AlN/Si substrates.

ABBREVIATIONS

TFET, tunnel field-effect transistors; SS, subthreshold slope; HS, heterostructure; vdW, van der Waals; TMDs, transition-metal dichalcogenides; BZ, Brillouin Zone; VBO, valence band offset; CBO, conduction band offset; Molecular Beam Epitaxy, MBE; van der Waals, vdW; X-ray photoelectron spectroscopy, XPS; Reflection high energy electron diffraction, RHEED; Angle-resolved photoelectron spectroscopy, ARPES; Perdew-Burke-Ernzerhof, PBE; Generalized-gradient approximation, GGA; Spin-orbit coupling (SOC);

Supporting Information:

Figure S1 Schematic representation of the structure of 1T-$SnSe_2$ crystal: (a) side view (b) top view. The unit cell contains only one layer.

Figure S2 DFT band structure calculations of (a) 4 ML 2H-$SnSe_2$ with D_{6h} (P63/mmc) symmetry and (b) 1ML orthorhombic SnSe (Pnma) phase free-standing slab with spin orbit coupling. DFT predicts that 2H-$SnSe_2$ is metallic in contrast to the case of 1T-$SnSe_2$ bandstructure where a semiconducting band gap of 0.4eV (GGA) was obtained (Fig. 3(c)). The orthorhombic SnSe band structure indicates a semiconductor material. Both phases in S2 (a) and (b) above are distinctly different from our experimentally derived $SnSe_2$band structure, presented in Fig. 3(a) in the main text. The corresponding Brillouin zone for $SnSe_2$ hexagonal (c) and SnSe orthorhombic (d) crystal lattices.

Figure S3 Enhanced contrast ARPES image of the valence band structure along the ΓM direction of the Brillouin zone for the 4 ML $SnSe_2/Bi_2Se_3$/AlN/Si(111) sample, the complete mapping of which is presented in Fig. 3(a) .The onset of the conduction band minimum is visible at the M point ($k_{x,//}$=0.9 $Å^{-1}$) and corresponds to the small peak near the Fermi level observed in the linescan (k_x=0.9 $Å^{-1}$) shown in Fig. 3(d). From S3 below, it can be seen that E_F is located at–or just above– the conduction band minimum indicating that the MBE-grown $SnSe_2$ is a strongly n-type material.

Figure S4 Schematic illustration of the proposed device layer structure consisting of the fully epitaxial 2D WSe_2/2D $SnSe_2/Bi_2Se_3$/AlN/Si(111) materials combination. As already mentioned in the main text, the Bi_2Se_3 buffer layer was introduced in order to achieve a good crystalline quality of the epilayers. However, since Bi_2Se_3 is conductive, it can serve as a bottom electrode in TFET device implementation. The structure in reverse order where WSe_2 is first grown followed by $SnSe_2$ top layer is also a suitable combination yielding similar band alignments. The final choice should be made taking into account layer stability in air and device processing flow.

[1] Ionescu, A.M. & Riel, H.; Tunnel field-effect transistors as energy efficient electronic switches. *Nature* **2011**, 479, 329-337.

[2] Lu, H. & Seabaugh, A.; Tunnel Field-Effect Transistors: State-of-the-Art. *J. EDS* **2014**, 2, 44-49.

[3] Koswatta, S. O.; Koester, S. J. and Haensch, W.; 1D Broken-gap Tunnel Transistor with MOSFET-like On-currents and Sub-60mV/dec Subthreshold Swing. *IEEE TED* **2010**, 57, 3222-3227.

[4] Sarkar, D.; Xie, X.; Liu, W.; Cao, W.; Kang, J.; Gong, Y.; Kraemer, S.; Ajayan, P. M. & Banerjee, K..; A subthermionic tunnel field-effect transistor with an atomically thin channel, *Nature* **2015**, 526, 91-95.

[5] Gong, C.; Zhang, H.; Wang, W.; Colombo, L.; Wallace, R. M. and Cho, K..; Band alignment of two dimensional transition metal dichalcogenides: Application in tunnel field effect transistors *Appl. Phys. Lett.* **2013**, 103, 053513.

[6] Aretouli, K. E.; Tsipas, P.; Tsoutsou, D.; Marquez-Velasco, J.; Xenogiannopoulou, E.; Giamini, S. A.; Vassalou, E.; Kelaidis, N. P.; Dimoulas, A. Two-Dimensional Semiconductor $HfSe_2$ and $MoSe_2/HfSe_2$ Van der Waals Heterostructures by Molecular Beam Epitaxy. *Appl. Phys. Lett.* **2015**, 106, 143105.

[7] Yue R.; Barton A. T.; Zhu H.;Azcatl A.; Pena L. F.; Wang J.;Peng X.; Lu N.; Cheng L.;Addou R.; McDonnell S.; Colombo L.; Hsu J. W. P.; Kim J.; Kim M. J.; Wallace R. M. and Hinkle C. L.; $HfSe_2$ Thin Films: 2D Transition Metal Dichalcogenides Grown by Molecular Beam Epitaxy. *ACS Nano* **2015**, 9, 474-480.

[8] Li, M.; Esseni, D.; Nahas, J. J.; Jena, D. and Xing, H. G.; Two-Dimensional Heterojunction Interlayer Tunneling Field Effect Transistors (Thin-TFETs). *J. EDS Soc.* **2015**, 3, 200-204.

[9] Schlaf, H.; Lang, G. O.; Pettenkofe,r C. and Jaegermann, W.; Band lineup of layered semiconductor heterointerfaces prepared by van der Waals epitaxy: Charge transfer correction term for the electron affinity rule *J. Appl. Phys.* **1999**, 85, 2732-2735.

[10] Yan, R.; Fathipour, S.; Han, Y.; Song, B.; Xiao, S.; Li, M.; Ma, N.; Protasenko, V.; Muller, D.A.; Jena, D. and Xing, H.C.; Esaki Diodes in van der Waals Heterojunctions with Broken-Gap Energy Band Alignment *Nanoletters* **2015**, 15, 5791-5798.

[11] Zhang, C.; Yin, H.; Han, M.; Dai, Z.; Pang, H.; Zheng, Y.; Lan, Y.; Bao, J. and Zhu, J.; Two-Dimensional Tin Selenide Nanostructures for Flexible All-Solid-State Supercapacitors. *ACS Nano* **2014**, 8, 3761-3770.

[12] Yu, P.; Yu, X.; Lu, W.; Lin, H.; Sun, L.; Du, K.; Liu, F.; Fu, W.; Zeng, Q.; Shen, Z.; Jin, C.; Wang, Q.Z. and Liu, Z., Fast Photoresponse from 1T Tin Diselenide Atomic Layers *Adv. Funct. Mater*. **2016**, 26, 137–145.

[13] Su, Y.; Ebrish, M.; Olson, E. J. & Koester, S. J. $SnSe_2$ field-effect transistors with high drive current. *Appl. Phys. Lett.* **2013**, 263104.

[14] Pei, T.; Bao, L.; Wang, G.; Ma, R.; Yang, H.; Li, J.; Gu, C.; Pantelides, S.; Du, S. and Gao, H.- J., Few-layer $SnSe_2$ transistors with high on/off ratios, *Appl. Phys. Lett.* **2016**, 108, 053506.

[15] Koma, A.; Ueno, K.; Saiki, K. Heteroepitaxial growth by Van der Waals interaction in one-, two- and three-dimensional materials. *J. Cryst. Growth* **1991**, 111, 1029−1032.

[16] Koma, A. and Yoshimura, K. Ultrasharp interfaces grown with Van der Waals epitaxy. *Surf. Sci.* **1986**, 174, 556−560.

[17] Schlaf, R.; Lang, O.; Pettenkofer, C.; Jaegermann, W. and Armstrong, N. R. Experimental determination of quantum dipoles at semiconductor heterojunctions prepared by van der Waals epitaxy: Linear correction term for the electron affinity rule, *Journal of Vacuum Science & Technology* **1997**, A15, 1365-1370

[18] Liu, H.; Jiao, L.; Xie, L.; Yang, F.; Chen, LJ.; Ho, W.K.; Gao C.L.; Jia, J.F.;Cui, X.D. and Xie, M.X.; Molecular beam epitaxy of monolayer and bilayer WSe_2: a scanning tunneling microscopy/spectroscopy study and deduction of exciton binding energy, *2D Mater.* **2015**, 2, 034004

[19] Liu, H.; Chen, J.; Yu, H.; Yang, F.; Jiao, L.; Liu, G.; Ho, W.; Gao, C.; Jia, J.; Yao W. and Xie M.; Observation of intervalley quantum interference in epitaxial monolayer tungsten diselenide, *Nat. Commun.* **2015**, DOI: 10.1038/ncomms9180

[20] Liu, H.; Jiao, L.; Yang, F.; Xie, L.; Cai, Y.; Wu, X.; Ho, W.; Gao, C.; Jia, J.; Wang, N.; Fan, H.; Yao, W. and Xie, M.; Dense Network of One-Dimensional Mid gap Metallic Modes in Monolayer $MoSe_2$ and Their Spatial Undulations *Phys. Rev. Lett.* **2014**, 113, 066105.

[21] Zhang, Y.; Chang, T.-R.; Zhou, B.; Cui, Y.-T.; Yan, H.; Liu, Z.; Schmitt, F.;Lee, J.; Moore, R.; Chen, Y.; Lin, H.;Jeng, H.; Mo, S.-K.; Hussain, Z.; Bansil, A; Shen, Z.-X.; Direct observation of the transition from indirect to direct bandgap in atomically thin epitaxial $MoSe_2$ *Nature Nanotech.*, **2014**, 9,111–115

[22] Vishwanath, S.; Liu ,X.; Rouvimov, S.; Mende, P.-C.; Azcatl, A.; McDonnell , S.; Wallace , R.W.; Feenstra, R.M.; Furdyna, J.; Jena, D. and Xing H.G.;"Comprehensive structural and optical characterization of MBE grown $MoSe_2$ on graphite, CaF_2 and graphene", *2D Mater.* **2015**, 2, 024007.

[23] Xenogiannopoulou, E.; Tsipas, P.; Aretouli, K. E.; Tsoutsou, D.; Giamini, S. A.; Bazioti, C.; Dimitrakopulos, G.P.; Komninou, Ph.; Brems, S.; Huyghebaert, C.; Radu, I. P. High-Quality, Large-Area $MoSe_2$ and $MoSe_2/Bi_2Se_3$Heterostructures on AlN(0001)/Si(111) Substrates by Molecular Beam Epitaxy. *Nanoscale* **2015**, 7, 7896-7905.

[24] Tsipas, P.; Tsoutsou, D.; Marquez-Velasco, J.; Aretouli, K. E.; Xenogiannopoulou, E.; Vassalou, E.; Kordas, G.; Dimoulas, A. Epitaxial $ZrSe_2/MoSe_2$ Semiconductor v.d. Waals

Heterostructures on Wide Band Gap AlN Substrates. *Microelectron. Eng.* **2015**, 147, 269-272.

[25] Tsoutsou, D.; Aretouli, K. E.; Tsipas, P.; Velasco, J.M.; Xenogiannopoulou, E.; Kelaidis, N.; Giamini, S. and Dimoulas, A.; Epitaxial 2D $MoSe_2$ ($HfSe_2$) semiconductor / 2D $TaSe_2$ metal v.d.Waals Heterostructures, *ACS Appl. Mater. Interf.* **2016,** 8, 1836-1841.

[26] Chattopadhyay, T.; Pannetier, J. and Von Schnering, H. G.;Neutron diffraction study of the structural phase transition in SnS and SnSe, *J. Phys. Chem. of Solids* **1986**, 47, 879-883.

[27] Wang, Z.; Wang, J.; Zang, Y.; Zhang, Q.; Shi, J.-A.; Jiang, T.; Gong, Y.; Song, C.-L.; Ji, S.-H.; Wang, L.-L.; Gu, L.; He, K.; Duan, W.; Ma, X.; Chen, X. and Xue, Q.-K.; Molecular Beam Epitaxy-Grown SnSe in the Rock-Salt Structure: An Artificial Topological Crystalline Insulator Material. *Adv. Mater.* **2015**, 27, 4150–4154.

[28] Huang, Y.; Xu, K.; Wang, Z.; Shifa, T.A,; Wang, Q.; Wang, F.; Jiang, C. and He, J.; Designing the shape evolution of $SnSe_2$ nanosheets and their optoelectronic properties, *Nanoscale* **2015,** 7**,**17375-17380.

[29] Boscher, N. D.; Carmalt, C.J.; Palgrave,R.G. and Parkin, I.P.; Atmospheric pressure chemical vapour deposition of SnSe and $SnSe_2$ thin films on glass, *Thin Solid films* **2008**,516 ,4750-4757.

[30] Ramasamy, P.; Manivasakan, P.and Kim, J.; Phase controlled synthesis of SnSe and $SnSe_2$ hierarchical nanostructures made of single crystalline ultrathin nanosheets, Cryst. Eng. Comm., **2015**, 17, 807-813.

[31] C. Zhang, C.; Yin, H.; Han, M.; Dai, Z.; Pang, H.; Zhang, Y.; Lan, Q.; Bao, J. and Zhu, J.; Two-Dimensional Tin Selenide Nanostructures for Flexible All-Solid-State Supercapacitors, *ACS Nano*, **2014**,8(4), 3761–3770.

[32] Perdew, J. P.; Wang, Y. Accurate and Simple Analytic Representation of the Electron-Gas Correlation Energy. *Phys. Rev. B: Condens. Matter Mater. Phys* .**1992**, 45, 13244.

[33] Perdew, J. P.; Burke, K.; and Ernzerhof, M.; Generalized Gradient Approximation Made Simple, *Phys. Rev. Lett.* **1996**, 77, 3865.

[34] Grimme, S.; Antony, J.; Ehrlich, S.; Krieg, S.A Consistent and Accurate Ab Initio Parametrization of Density Functional Dispersion Correction (DFT-D) for the 94 Elements H-Pu. *J. Chem. Phys.* **2010**, 132, 154104.

[35] Chadi, D. J.; Cohen, M. L. Special Points in the BrillouinZone. *Phys. Rev. B: Condens. Matter Mater. Phys.* **1973**, 8, 5747.

[36] Huang, J.K.; Pu, J.; Hsu,C.-L.; Chiu, M.-H.; Juang, Z-Y.; Chang, Y.-H.; Chang, W.-H.; Iwasa, Y.; Takenobu, T.; and Li, L.-J.; Large-Area Synthesis of Highly Crystalline WSe_2 Monolayers and Device Applications. *ACS Nano* **2014**, 8, 923-930.

[37] Akintola, K.; Andrews, G.T.;Curnoe, S.H.; Koehler, M.R; and Keppens, V.; Raman and Brillouin scattering studies of bulk 2H-WSe_2 .*J. Phys. Cond.Mat.* **2015**, 27395401

[38] Tsipas, P.; Xenogiannopoulou, E.; Kassavetis, S.; Tsoutsou, D.; Golias, E.; Bazioti, C.; Dimitrakopulos, G.P.; Komninou, Ph.; Liang, H.; Caymax, M.; and Dimoulas, A.; Observation of Surface Dirac Cone in High Quality Ultrathin Epitaxial Bi_2Se_3 Topological Insulator on AlN(0001) Dielectric. *ACS Nano*, **2014**, *8* (7), 6614–6619.

[39] Palosz B,; Salje E.; Lattice parameters and spontaneous strain in AX_2polytypes Cdl_2, Pbl_2, SnS_2 and $SnSe_2$. *J Appl. Crystallogr.*, **1989**, 22(6), 622.

[40] Agarwal, M. K.; Wani, P. A. Growth conditions and crystal structure parameters of layer compounds in the series $Mo_{1-x}W_xSe_2$. *Materials Research Bulletin* **(1979)** 14 (6), 825–830.

[41] Julien, C.; Eddrief, M.; Samaras, I.; and M. Balkanski,; Optical and electrical characterizations of SnSe, SnS_2 and $SnSe_2$ single crystals. *Mater. Sci. Eng. B*, **1992**, 15, 70-72.

[42] Bhatt, V. P. and Gireesan, K.; Influence of heat treatment on electrical properties of thermally evaporated tin diselenide ($SnSe_2$) thin films. *Journal of Materials Science Materials in Electronics* **1991**, 2, 4-6.

[43] Borges, Z.V.; Poffo, C.M.; de Lima, J.C.; de Souza, S.M.; Triches, D.M.; Nogueira, T.P.O.; Manzato, L.; de Biasi, R.S.; Study of structural, optical and thermal properties of nanostructured $SnSe_2$ prepared by mechanical alloying. *Materials Chemistry and Physics* **2016,** 169, 47-54

[44] Non-Tetrahedrally Bonded Elements and Binary Compounds I, edited by O. Madelung, U. Roossler, and M. Schulz (Springer, Berlin, Heidelberg, 1998), Vol. 41C, Chap. 801, p. 1.

[45] Kraut, E.; Grant, R.; Waldrop, J.; and Kowalczyk, S.; Precise Determination of the Valence-Band Edge in X-Ray Photoemission Spectra: Application to Measurement of Semiconductor Interface Potentials. *Phys. Rev. Lett.* **1980,** 44**,** 1620.

[46] Liu, W.; Cao, W.; Kang, J.; and K. Banerjee, K.; High- Performance Field-Effect-Transistors on Monolayer WSe_2.*ECS Transactions* **2013,** 58(7) 281-285.

[47] Sahin, H.; Tongay, S.; Horzum, S.; Fan, W.; Zhou, J.; Li, J.; Wu, J.; and Peeters, F.M., Anomalous Raman Spectra and Thickness Dependent Electronic properties of WSe_2. *Phys. Rev. B* **2013,** 87, 165409.

FIGURES

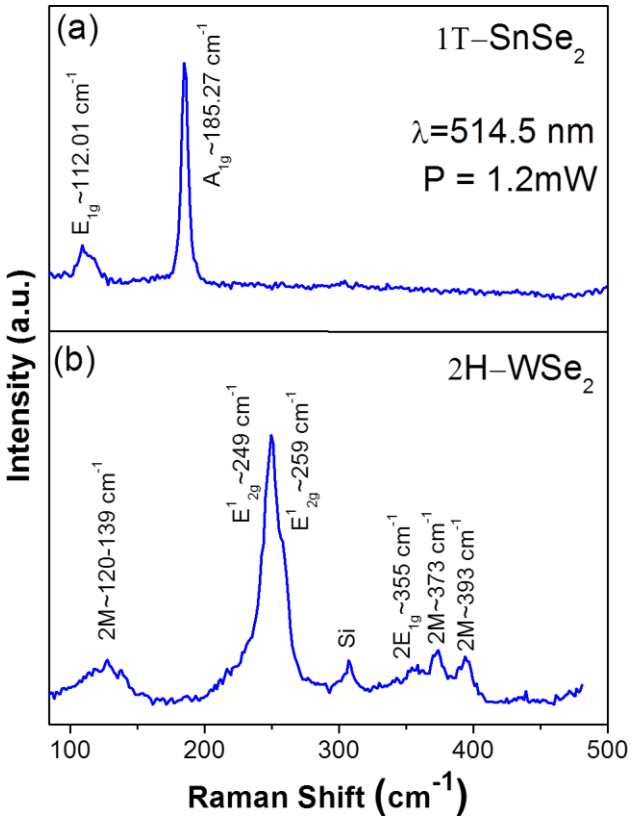

Figure 1: Raman spectrum of the MBE deposited $SnSe_2$ and WSe_2 samples. Fig. 1(a) shows the two characteristic peaks at 186.27cm^{-1} and 112 cm^{-1}corresponding to the A_{g1} and E_g active modes of 1T-$SnSe_2$. Fig.1 (b) shows two pronounced peaks at 249 and 259 cm^{-1} which correspond to E^1_{2g} (in-plane) and A_{1g} (out of plane) modes of 2H-WSe_2 and a number of second order (2M) peaks. A peak arising from the Si substrate is also visible.

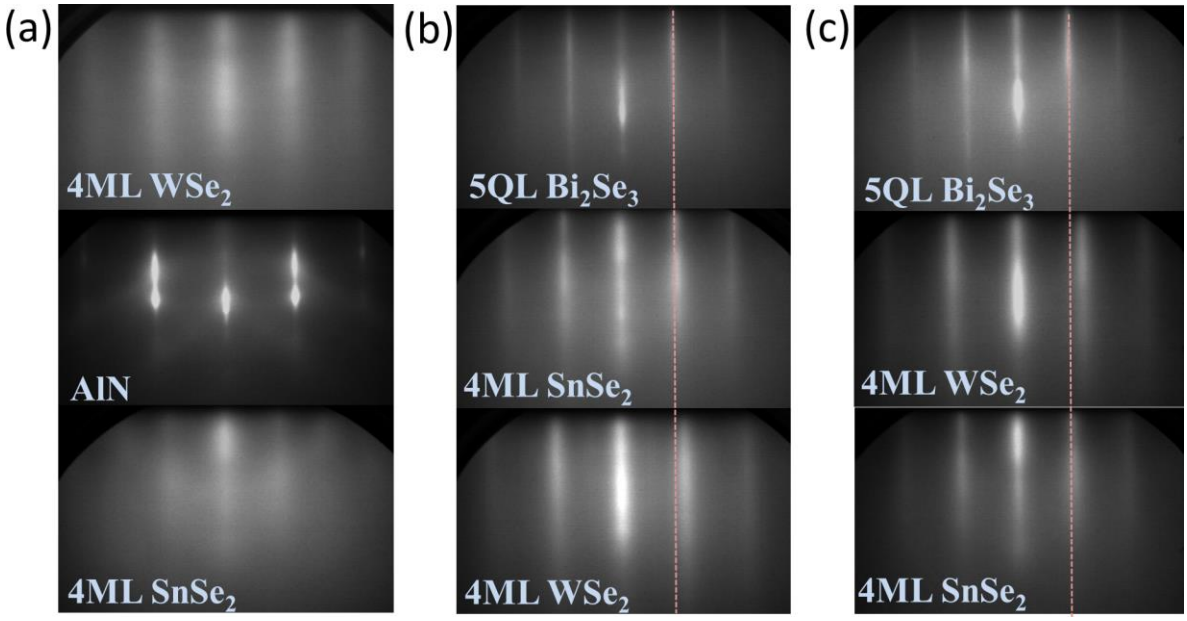

Figure 2: RHEED patterns along [11-20] azimuth of (a) 4ML WSe_2/AlN(0001)/Si(111) (top) and 4ML $SnSe_2$/AlN/Si(111) (bottom) grown separately on AlN substrates (middle), (b) 5QL Bi_2Se_3/AlN (top), 4ML $SnSe_2$/Bi_2Se_3 (middle) showing improved crystal quality and 4ML WSe_2/$SnSe_2$ (bottom), (c) 5QL Bi_2Se_3/AlN, 4ML WSe_2/Bi_2Se_3 (middle) and 4ML $SnSe_2$/WSe_2 (bottom). Despite the large lattice mismatch between the different epitaxial layers and the substrate, all RHEED streaks are azimuthially aligned in the plane.

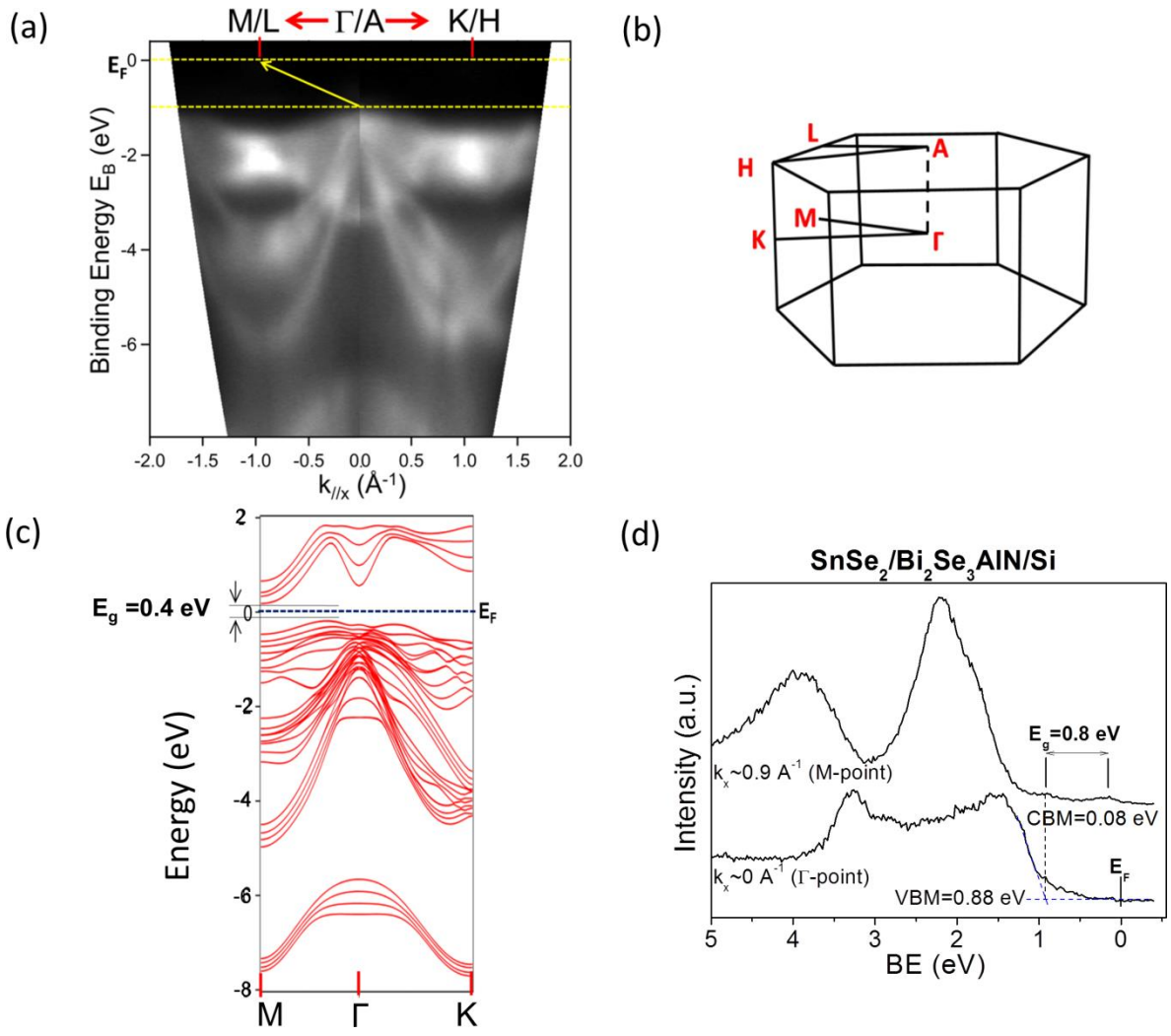

Figure 3: (a) ARPES valence band imaging using He I excitation of 21.22 eV along the high symmetry directions K/H-Γ/A-M/L of the Brillouin zone for a 4 ML $SnSe_2/Bi_2Se_3/AlN/Si(111)$ sample. The arrow indicates the indirect gap from Γ point (experimental maximum of the valence band) to M-point (minimum of conduction band), (b) Brillouin zone for hexagonal lattice system, (c) DFT band structure calculations of 4 ML $SnSe_2$ free-standing slab with spin orbit coupling and (d) line scans of the $SnSe_2/Bi_2Se_3/AlN/Si(111)$ sample, recorded at both the Γ (k_x=0) and M-(k_x=0.9Å^{-1}) points of the surface BZ. E_g is the indirect energy gap while CBM and VBM denote the conduction band minimum and valence band maximum, respectively.

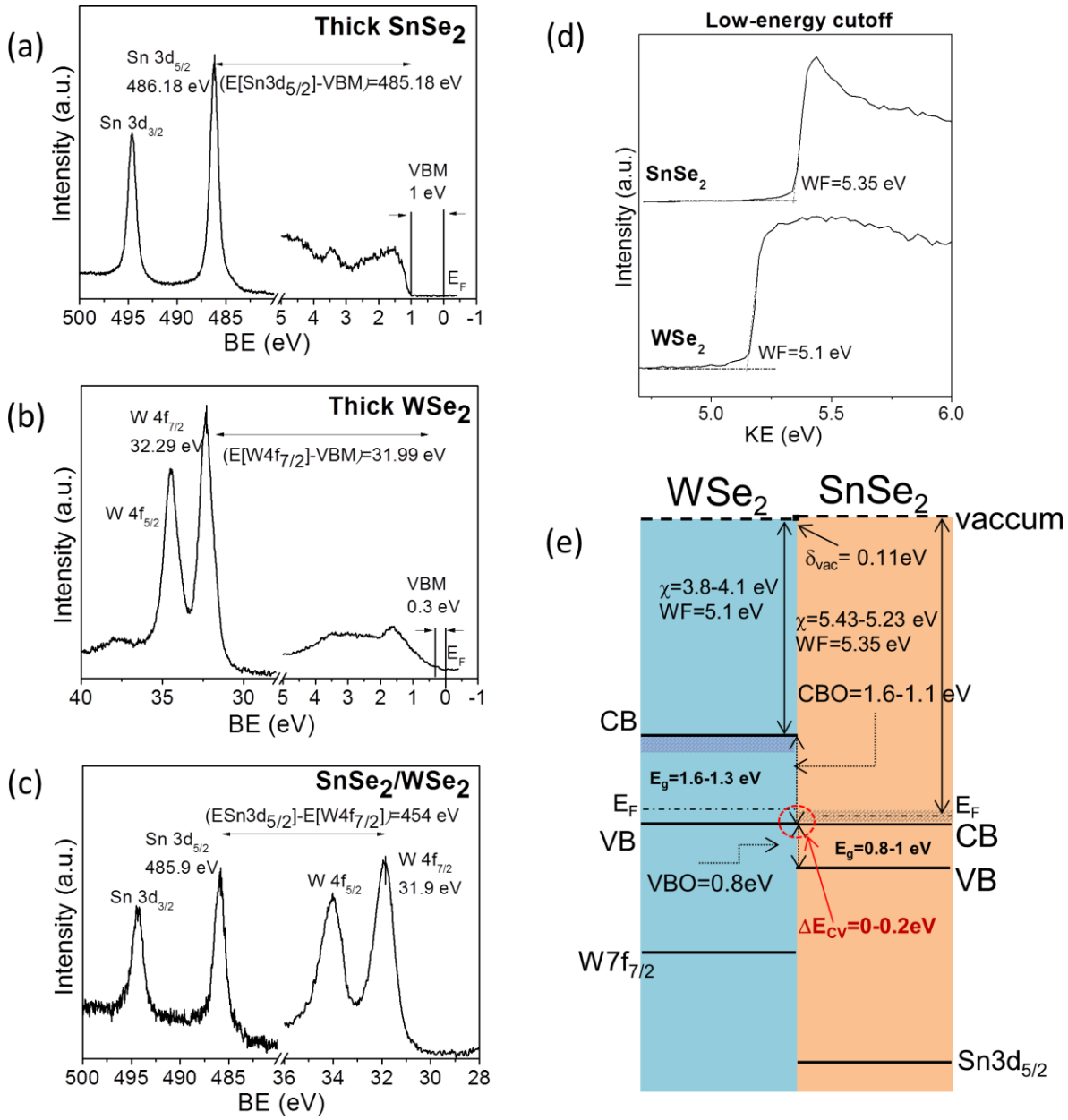

Figure 4: Band alignment of the $WSe_2/SnSe_2$ heterostructure (a) XPS of thick $SnSe_2$, (b) XPS of thick WSe_2 and (c) XPS of thin $SnSe_2/WSe_2$ samples, (d) Low-energy electron cut off for the epitaxially grown $SnSe_2$ and WSe_2 samples, as deduced from UPS spectra, (e) Schematic of the $WSe_2/SnSe_2$ band alignments as reconstructed by XPS core level analysis. χ and E_F denote the electron affinity and the Fermi energy, respectively. E_g is the energy gap while CBO and VBO denote the conduction and valence band offsets, respectively. The shaded areas denote the energy range of variation of the conduction band minimum in both materials due to the different reported E_g values in the literature.

Graphical abstract